Supplementary Information

Decoding Mixed-Ion Effects in Halide Electrolytes: Entropy as a Unified Measure of Soft and Disordered Lattice

Renyu Cai [a], Yu Yang [b], Hong Zhu [a, *]

a. Global College, Shanghai Jiao Tong University, Shanghai 200240, China

b. Institute of Future Technology, Southwest Jiaotong University, Chengdu 611756, China

*Corresponding author:

E-mail: hong.zhu@sjtu.edu.cn

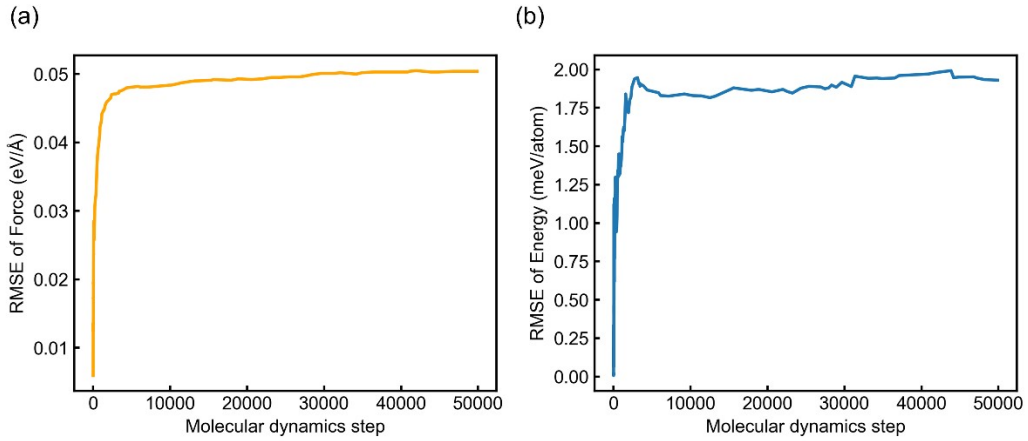

Figure S1: An evolution of the root mean square error (RMSE) of (a) force and (b) energy for molecular dynamic simulation of Li_3ScCl_6 at 1000K.

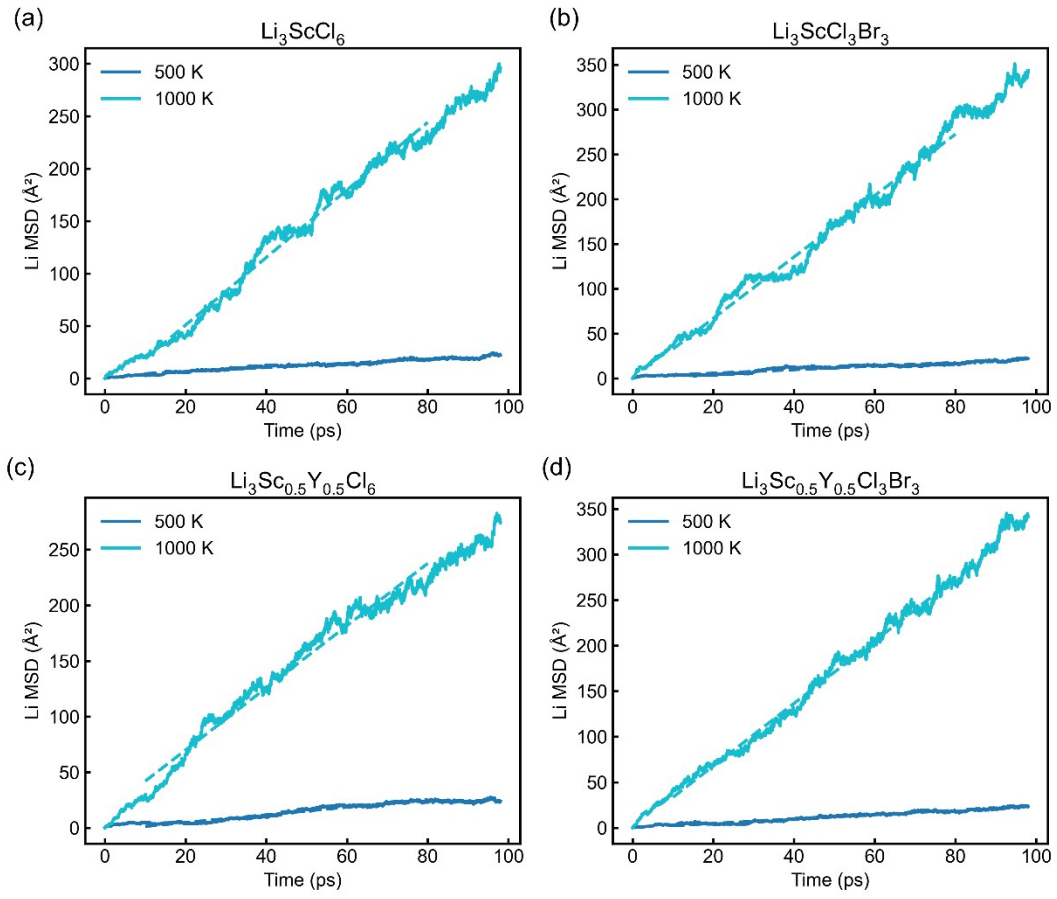

Figure S2: Li MSD curves obtained from MD simulations for 4 representative halides at 500K and 1000K, demonstrating consistent fitted diffusivities and reliable convergence.

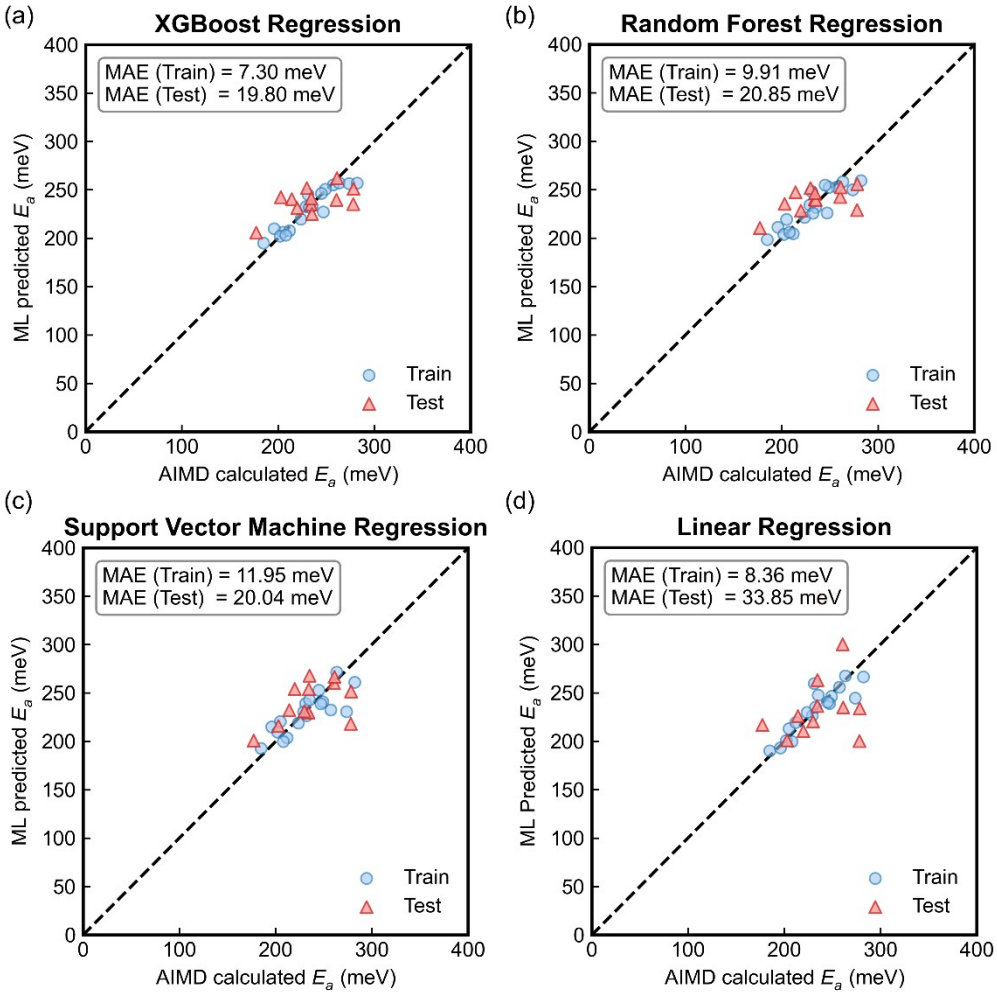

Figure S3: Performance comparison of four machine learning algorithms for predicting the activation energy (E_a) of Li-ion diffusion. The parity plots display the AIMD-calculated values versus the machine learning predicted values for (a) XGBoost (b) random forest, (c) support vector machine (SVM), and (d) Linear Regression The dashed diagonal lines represent the ideal prediction. The mean absolute error (MAE) for both training and test sets is inset in each panel.

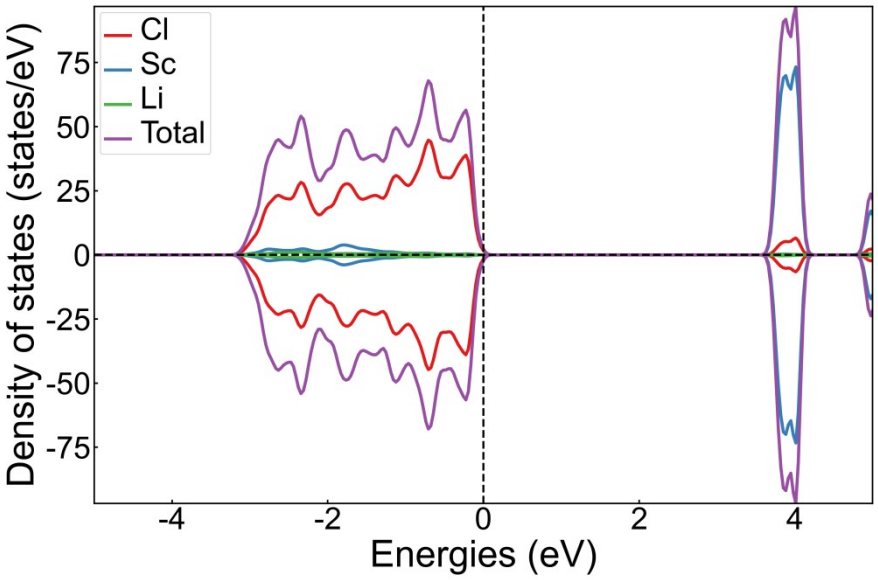

Figure S4: Calculated electronic density of states (DOS) for the prototype Li_3ScCl_6. The energy scale is aligned to the valence band maximum (VBM) at 0 eV. The projected DOS (PDOS) analysis reveals that the VBM is predominantly governed by the Cl 3p orbitals, while the conduction band minimum (CBM) is mainly derived from the Sc 3d states. This indicates that the intrinsic electrochemical oxidation and reduction limits are dictated by the anion framework and the transition metal cation, respectively.

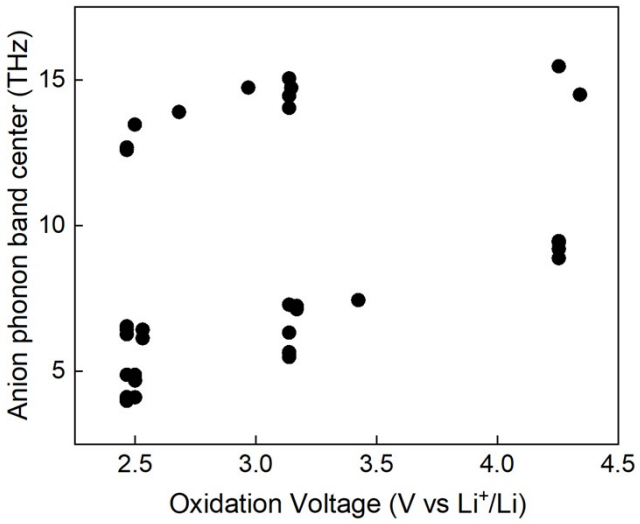

Figure S5: Correlation between computed stability oxidation potential with the computed anion band center of halides.

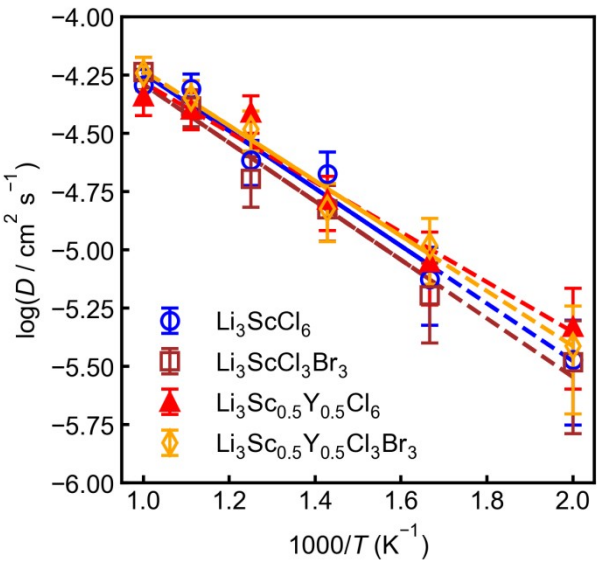

Figure S6: Arrhenius plots of Li^+ diffusivity from AIMD simulations for the representatives of the eight identified candidates.

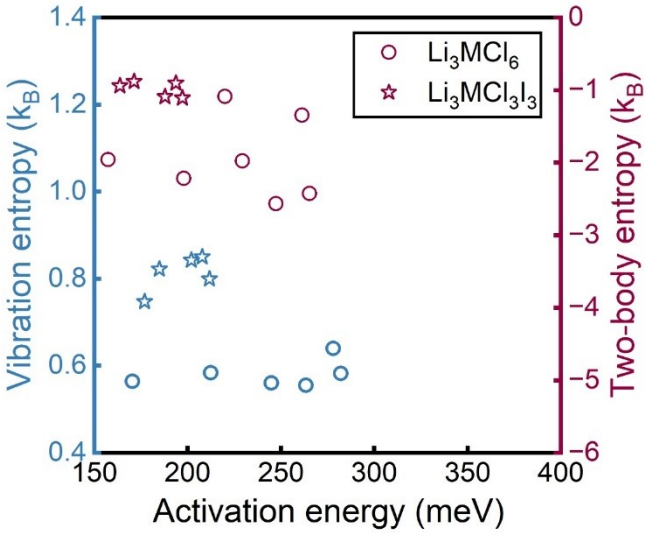

Figure S7: Comparison of the Li diffusion activation energy between single-anion and anion-mixed halides. The circles represent single-anion systems (Li_3MCl_6, M= Sc, $Sc_{0.5}In_{0.5}$, In, $Sc_{0.5}Y_{0.5}$, $In_{0.5}Y_{0.5}$, Y), while the stars denote anion-mixed systems ($Li_3MCl_3I_3$, M= Sc, $Sc_{0.5}In_{0.5}$, In, $Sc_{0.5}Y_{0.5}$, $In_{0.5}Y_{0.5}$, Y). The anion-mixed halides exhibit a remarkably lower average activation energy of 0.20 eV compared to their single-anion counterparts (0.24 eV), highlighting the entropy-driven enhancement of Li-ion diffusion.

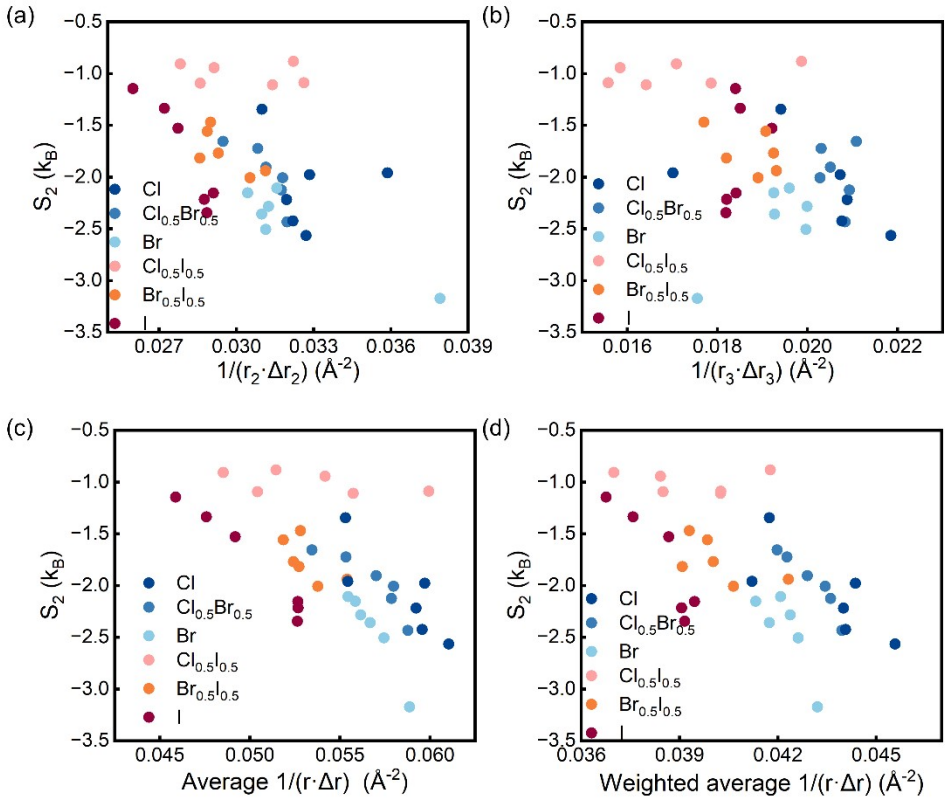

Figure S8: Correlation between the two-body entropy (S_2) and the product of (a) the 2nd Li-Li RDF peak radial distance (r_2) and the integral breadth (Δr_2), (b) the 3rd Li-Li RDF peak radial distance (r_3) and the integral breadth (Δr_3), (c) the average $1/(r\cdot\Delta r)$ of the 1st, 2nd, and 3rd RDF peaks ($\frac{1}{3}(\frac{1}{r_1\cdot\Delta r_1}+\frac{1}{r_2\cdot\Delta r_2}+\frac{1}{r_3\cdot\Delta r_3})$), (d) the weighted average $1/(r\cdot\Delta r)$ of the 1st, 2nd, and 3rd RDF peaks ($\frac{\Delta r_1}{\Delta r_1+\Delta r_2+\Delta r_3}\cdot\frac{1}{r_1\Delta r_1}+\frac{\Delta r_2}{\Delta r_1+\Delta r_2+\Delta r_3}\cdot\frac{1}{r_2\Delta r_2}+\frac{\Delta r_3}{\Delta r_1+\Delta r_2+\Delta r_3}\cdot\frac{1}{r_3\Delta r_3}$)

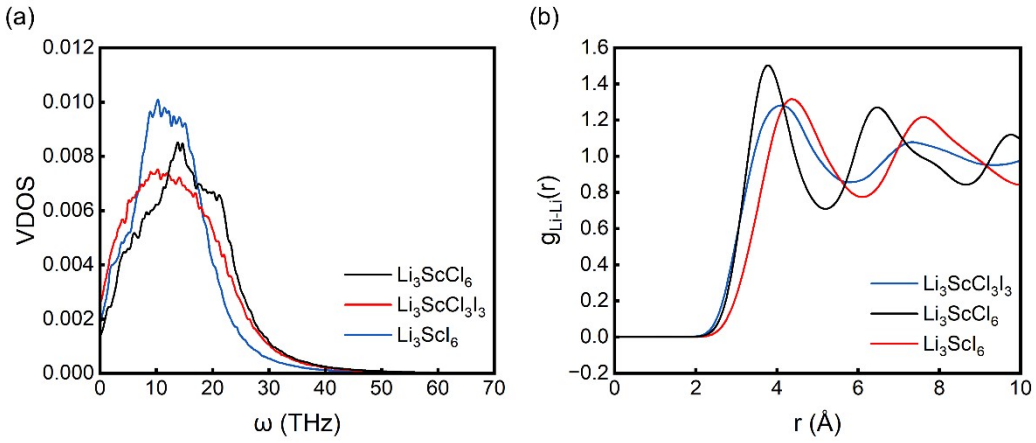

Figure S9: (a) Li-ion phonon DOS and (b) Li-Li radial distribution functions for Li_3ScCl_6, Li_3ScI_6 and $Li_3ScCl_3I_3$ at 1000 K.

(a)

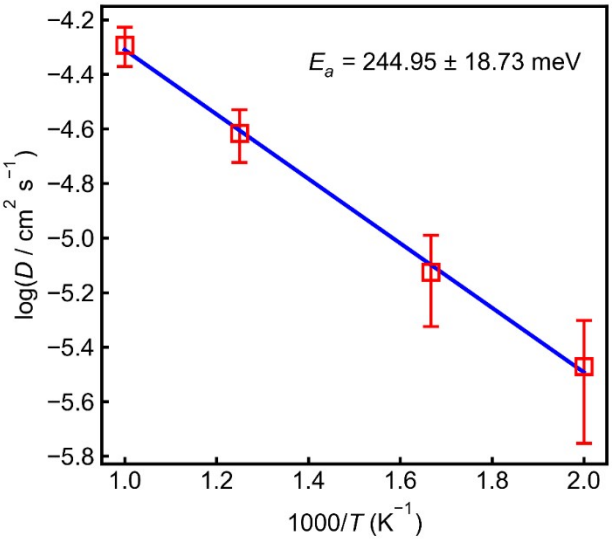
E_a = 244.95 ± 18.73 meV
log(D / cm^2 s^{-1})
−4.2
−4.4
−4.6
−4.8
−5.0
−5.2
−5.4
−5.6
−5.8
1.0
1.2
1.4
1.6
1.8
2.0
1000/T (K^{-1})

(b)

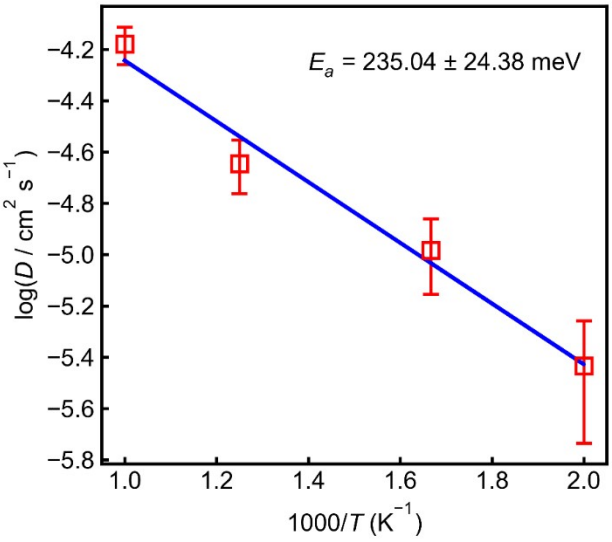
E_a = 235.04 ± 24.38 meV
log(D / cm^2 s^{-1})
−4.2
−4.4
−4.6
−4.8
−5.0
−5.2
−5.4
−5.6
−5.8
1.0
1.2
1.4
1.6
1.8
2.0
1000/T (K^{-1})

(c)

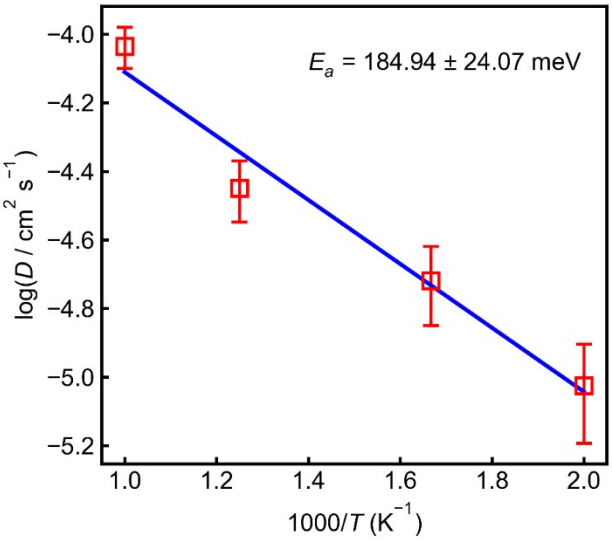

Figure S10: Arrhenius plots of Li-ion diffusion coefficients derived from AIMD simulations. The data points represent the calculated diffusivities at different temperatures, and the solid lines indicate the linear fits according to the Arrhenius equation. The calculated activation energy (E_a) is labeled for each composition (a) Li_3ScCl_6, (b)Li_3ScI_6, (c)$Li_3ScCl_3I_3$.

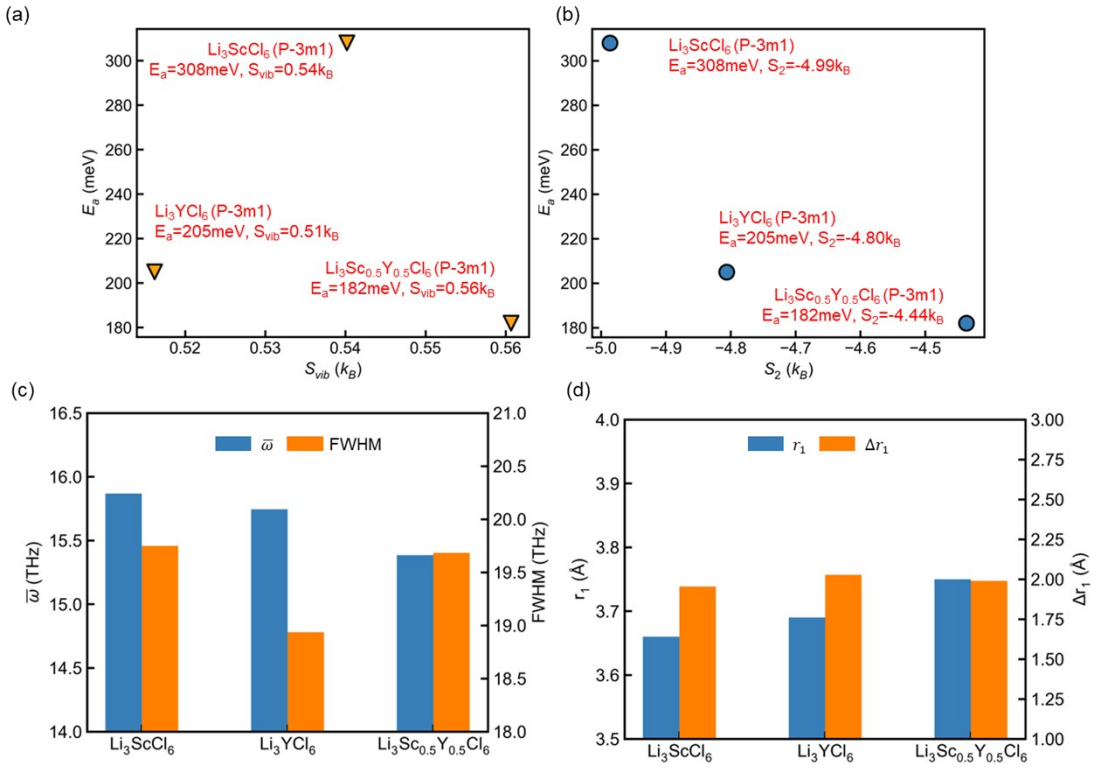

Figure S11: (a-b) Comparison of activation energy of Li-ion diffusion (E_a) and the entropy (S_{vib}, S_2) for P-3m1 halides (Li_3ScCl_6, Li_3YCl_6, $Li_3Sc_{0.5}Y_{0.5}Cl_6$) (c-d) Trends in the primary descriptors for vibrational entropy ($\bar{\omega}$, $FWHM$) and two-body entropy (r_1, Δr_1) across the Li_3ScCl_6, Li_3YCl_6, and $Li_3Sc_{0.5}Y_{0.5}Cl_6$.

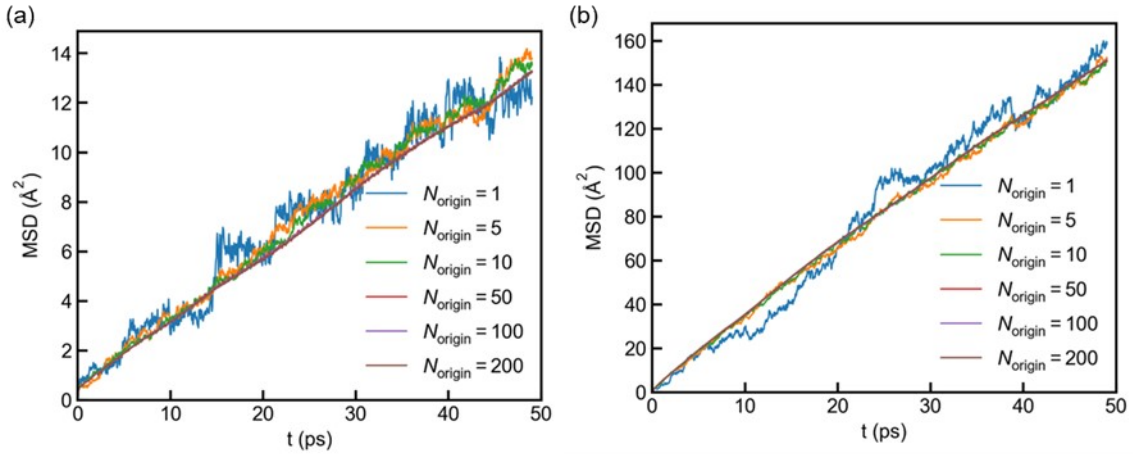

Figure S12: The calculated Li MSD with different number of time origins (N_{origin}) in Li_3ScCl_6 (a) at 500K and (b) at 1000K.

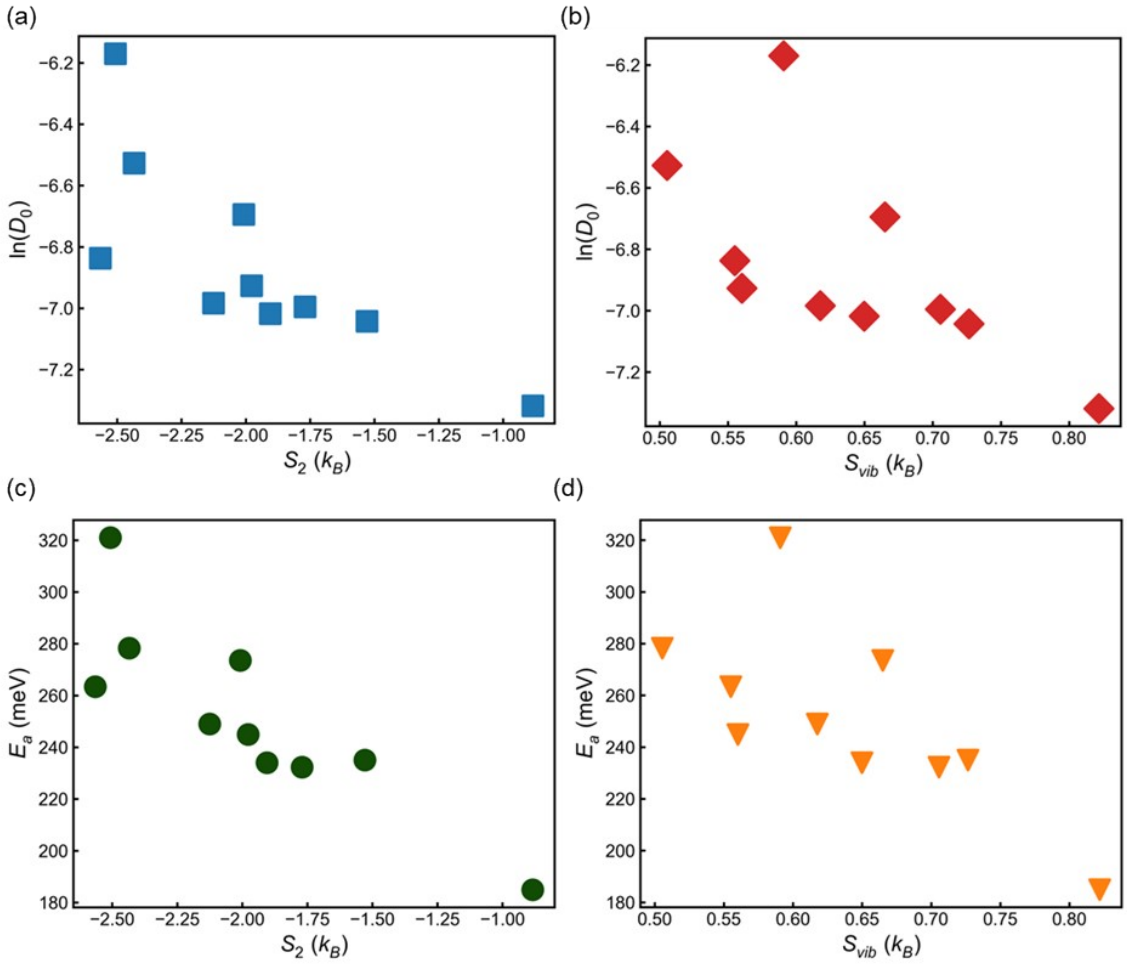

Figure S13: (a-b) Comparison of natural logarithm of pre-index factor of ion diffusion coefficient (lnD_0) and the entropy (S_{vib}, S_2) for C2/m halides (c-d) Comparison of the activation energy of Li-ion diffusion and the entropy for C2/m halides.

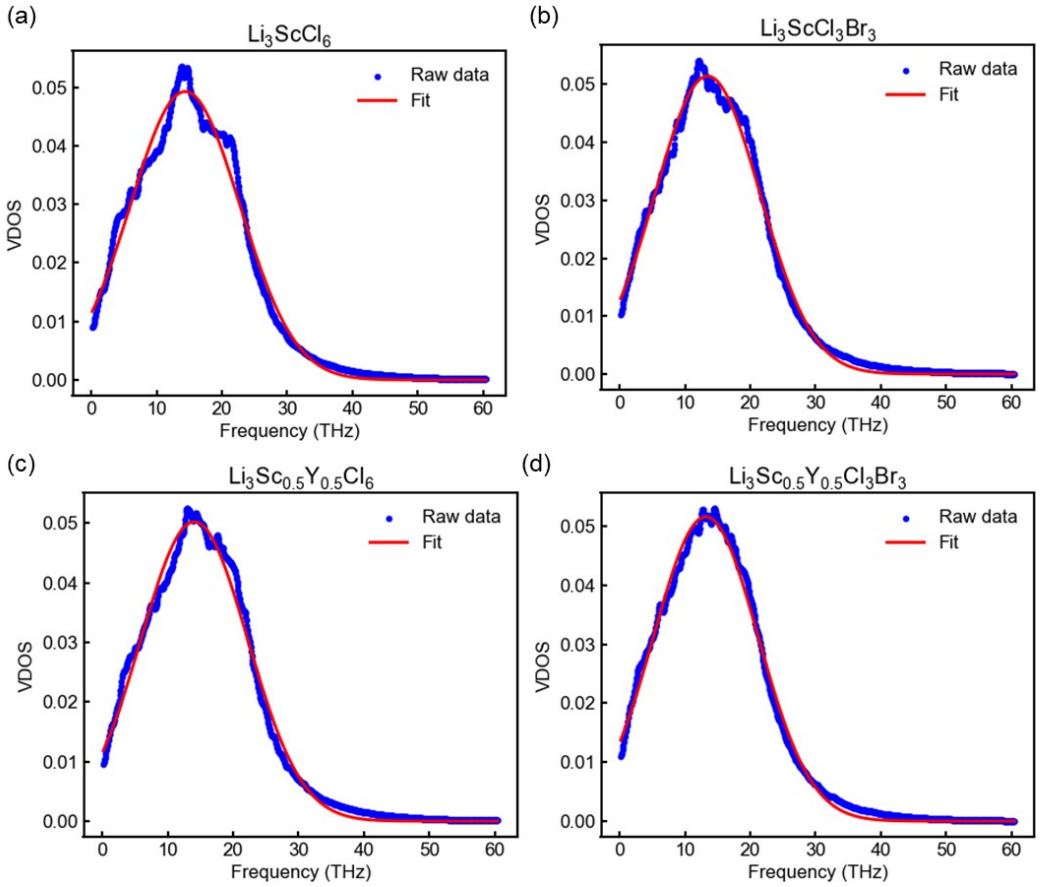

Figure S14: Comparison of the fitted curves with the raw VDOS profiles from MD simulations for 4 representative halides at 1000 K.

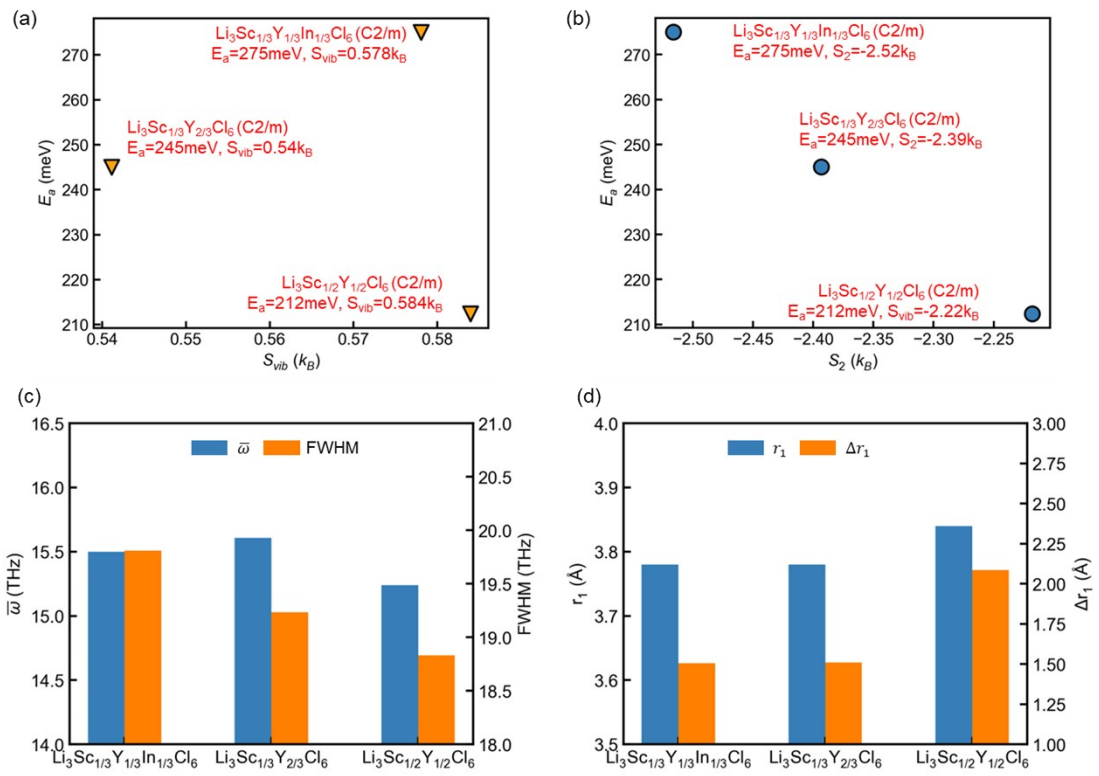

Figure S15: (a-b) Comparison of activation energy of Li-ion diffusion (E_a) and the entropy (S_{vib}, S_2) for C2/m halides ($Li_3Sc_{1/2}Y_{1/2}Cl_6$, $Li_3Sc_{1/3}Y_{2/3}Cl_6$, $Li_3Sc_{1/3}Y_{1/3}In_{1/3}Cl_6$) (c-d) Trends in the primary descriptors for vibrational entropy ($\bar{\omega}$, $FWHM$) and two-body entropy (r_1, Δr_1) across the halides.

Table S1: lattice parameters of Li_3MX_6 (M=Sc, $Sc_{0.5}In_{0.5}$, In, $Sc_{0.5}Y_{0.5}$, $In_{0.5}Y_{0.5}$, Y, X=Cl, $Cl_{0.5}Br_{0.5}$, Br, $Cl_{0.5}I_{0.5}$, $Br_{0.5}I_{0.5}$, I) computed by DFT.

Halides	a(Å)	b(Å)	c(Å)	α(°)	β(°)	γ(°)
Li_3ScCl_6	6.4260	11.0407	19.2917	90.00	108.17	90.00
Li_3YCl_6	6.5984	11.3938	19.5294	90.00	108.50	90.00
Li_3InCl_6	6.4607	11.1892	19.4053	90.00	108.03	90.00
Li_3ScBr_6	6.8211	11.7233	20.4887	90.00	107.86	90.00
Li_3YBr_6	6.9611	12.0162	20.7585	90.00	107.78	90.00
Li_3InBr_6	6.8415	11.8768	20.6494	90.00	107.70	90.00
Li_3ScI_6	7.3975	12.7157	22.3026	90.00	108.00	90.00
Li_3YI_6	7.5022	12.9836	22.5732	90.00	107.95	90.00
Li_3InI_6	7.4100	12.9050	22.4123	90.00	107.76	90.00
$Li_3ScCl_3Br_3$	6.6462	11.3905	20.0233	90.05	108.64	89.94
$Li_3YCl_3Br_3$	6.8510	11.7390	20.2529	90.21	106.45	89.69
$Li_3InCl_3Br_3$	6.6830	11.5277	20.1464	90.13	108.63	90.06
$Li_3ScCl_3I_3$	7.0811	12.3740	20.8828	88.07	105.69	88.92
$Li_3YCl_3I_3$	7.3110	12.5654	21.3061	89.68	108.56	91.75
$Li_3InCl_3I_3$	7.0519	12.4922	20.9750	89.37	106.15	89.92
$Li_3ScBr_3I_3$	7.1417	12.3113	21.4584	90.31	108.41	90.27
$Li_3YBr_3I_3$	7.2865	12.5350	21.7948	90.40	108.53	90.11
$Li_3InBr_3I_3$	7.1727	12.4933	21.5085	89.69	107.88	89.70
$Li_3Sc_{0.5}In_{0.5}Cl_6$	6.5278	11.2271	19.3986	90.00	107.89	90.00
$Li_3Sc_{0.5}Y_{0.5}Cl_6$	6.4533	11.0598	19.4357	90.00	109.26	90.00
$Li_3Y_{0.5}In_{0.5}Cl_6$	6.5678	11.2511	19.4374	90.00	109.03	90.00
$Li_3Sc_{0.5}In_{0.5}Br_6$	6.8570	11.8548	20.8341	90.00	108.78	90.00
$Li_3Sc_{0.5}Y_{0.5}Br_6$	6.8274	11.8195	20.6330	90.00	108.47	90.00
$Li_3Y_{0.5}In_{0.5}Br_6$	6.8827	11.9709	20.7743	90.00	108.52	90.00
$Li_3Sc_{0.5}In_{0.5}I_6$	7.4165	12.8258	22.5884	90.00	108.45	90.00
$Li_3Sc_{0.5}Y_{0.5}I_6$	7.4179	12.7202	22.5142	90.00	108.83	90.00

$Li_3Y_{0.5}In_{0.5}I_6$	7.4921	12.8640	22.5995	90.00	108.86	90.00
$Li_3Sc_{0.5}In_{0.5}Cl_3Br_3$	6.7823	11.5447	20.1076	90.37	108.39	90.35
$Li_3Sc_{0.5}Y_{0.5}Cl_3Br_3$	6.6711	11.4317	20.0818	89.85	109.15	89.93
$Li_3In_{0.5}Y_{0.5}Cl_3Br_3$	6.7726	11.6612	20.2365	90.22	106.54	89.97
$Li_3Sc_{0.5}In_{0.5}Cl_3I_3$	7.1706	12.5575	20.7029	90.00	105.35	90.00
$Li_3Sc_{0.5}Y_{0.5}Cl_3I_3$	7.0894	12.2916	21.1836	90.39	107.48	91.18
$Li_3In_{0.5}Y_{0.5}Cl_3I_3$	7.1819	12.4579	21.1515	90.13	108.19	88.73
$Li_3Sc_{0.5}In_{0.5}Br_3I_3$	7.2402	12.4050	21.6227	89.72	108.02	89.95
$Li_3Sc_{0.5}Y_{0.5}Br_3I_3$	7.1457	12.3697	21.4950	89.50	107.53	89.93
$Li_3In_{0.5}Y_{0.5}Br_3I_3$	7.2187	12.4838	21.7169	89.96	108.36	90.24

Table S2: Energy above hull for Li_3MX_6 (M=Sc, Y, In, $Sc_{0.5}In_{0.5}$, $Sc_{0.5}Y_{0.5}$, $In_{0.5}Y_{0.5}$, X=Cl, Br, I, $Cl_{0.5}Br_{0.5}$, $Cl_{0.5}I_{0.5}$, $Br_{0.5}I_{0.5}$) computed by DFT.

Halides	Energy above hull(eV)
Li_3ScCl_6	23
Li_3YCl_6	32
Li_3InCl_6	0
Li_3ScBr_6	0
Li_3YBr_6	32
Li_3InBr_6	24
Li_3ScI_6	4
Li_3YI_6	35
Li_3InI_6	35
$Li_3ScCl_3Br_3$	28
$Li_3YCl_3Br_3$	40
$Li_3InCl_3Br_3$	55
$Li_3ScCl_3I_3$	45
$Li_3YCl_3I_3$	62
$Li_3InCl_3I_3$	110
$Li_3ScBr_3I_3$	17
$Li_3YBr_3I_3$	47
$Li_3InBr_3I_3$	70
$Li_3Sc_{0.5}In_{0.5}Cl_6$	5
$Li_3Sc_{0.5}Y_{0.5}Cl_6$	27
$Li_3Y_{0.5}In_{0.5}Cl_6$	4
$Li_3Sc_{0.5}In_{0.5}Br_6$	11
$Li_3Sc_{0.5}Y_{0.5}Br_6$	19
$Li_3Y_{0.5}In_{0.5}Br_6$	30
$Li_3Sc_{0.5}In_{0.5}I_6$	19
$Li_3Sc_{0.5}Y_{0.5}I_6$	23
$Li_3Y_{0.5}In_{0.5}I_6$	32
$Li_3Sc_{0.5}In_{0.5}Cl_3Br_3$	46
$Li_3Sc_{0.5}Y_{0.5}Cl_3Br_3$	34
$Li_3In_{0.5}Y_{0.5}Cl_3Br_3$	47
$Li_3Sc_{0.5}In_{0.5}Cl_3I_3$	79
$Li_3Sc_{0.5}Y_{0.5}Cl_3I_3$	55
$Li_3In_{0.5}Y_{0.5}Cl_3I_3$	73
$Li_3Sc_{0.5}In_{0.5}Br_3I_3$	51
$Li_3Sc_{0.5}Y_{0.5}Br_3I_3$	29
$Li_3In_{0.5}Y_{0.5}Br_3I_3$	46

Table S3: Electrochemical stability window of Li_3MX_6 including phase equilibria at reduction and oxidation potentials.

Halides	Reduction Potential (V)	Phase equilibria at the reduction potential	Oxidation Potential (V)	Phase equilibria at the oxidation potential
Li_3ScCl_6	0.91	$ScCl_3$, LiCl	4.25	$ScCl_3$, Cl_2
Li_3YCl_6	0.65	YCl_3, LiCl	4.25	YCl_3, Cl_2
Li_3InCl_6	2.51	Li_3InCl_6	4.34	$InCl_3$, Cl_2
Li_3ScBr_6	0.90	$ScBr_3$, LiBr	3.15	$ScBr_3$, Br
Li_3YBr_6	0.59	YBr_3, LiBr	3.14	YBr_3, Br
Li_3InBr_6	2.17	$InBr_3$, LiBr	3.14	$InBr_3$, Br
Li_3ScI_6	1.11	ScI_3, LiI	2.47	ScI_3, I
Li_3YI_6	0.55	YI_3, LiI	2.47	YI_3, I
Li_3InI_6	1.98	$LiInI_4$, LiI	2.47	$LiInI_4$, I
$Li_3ScCl_3Br_3$	0.91	LiBr, $ScCl_3$	3.14	$ScCl_3$, Br
$Li_3YCl_3Br_3$	0.59	LiCl, YBr_3	3.17	YCl_3, Br
$Li_3InCl_3Br_3$	2.17	$InBr_3$, LiCl	3.42	Li_3InCl_6, $InBr_3$, Br
$Li_3ScCl_3I_3$	0.97	$ScCl_3$, LiI	2.47	$ScCl_3$, I
$Li_3YCl_3I_3$	0.59	LiCl, YI_3	2.53	YCl_3, I
$Li_3InCl_3I_3$	2.04	InI_3, LiCl	2.97	Li3$InCl_6$, InI_3, I
$Li_3ScBr_3I_3$	1.11	LiBr, ScI_3	2.50	$ScBr_3$, I
$Li_3YBr_3I_3$	0.55	LiBr, YI_3	2.50	YBr_3, I
$Li_3InBr_3I_3$	2.04	InI_3, LiBr	2.68	$InBr_3$, I
$Li_3Sc_{0.5}In_{0.5}Cl_6$	2.63	Li_3InCl_6, $ScCl_3$, LiCl	4.25	Li_3InCl_6, $ScCl_3$, Cl_2
$Li_3Sc_{0.5}Y_{0.5}Cl_6$	0.91	$ScCl_3$, YCl_3, LiCl	4.25	$ScCl_3$, YCl_3, Cl_2
$Li_3Y_{0.5}In_{0.5}Cl_6$	2.63	LiCl, Li_3InCl_6,	4.25	Li_3InCl_6, YCl_3, Cl_2

		YCl_3		
$Li_3Sc_{0.5}In_{0.5}Br_6$	2.17	$InBr_3$, $ScBr_3$, LiBr	3.14	$InBr_3$, $ScBr_3$, Br
$Li_3Sc_{0.5}Y_{0.5}Br_6$	0.91	$ScBr_3$, YBr_3, LiBr	3.14	$ScBr_3$, YBr_3, Br
$Li_3Y_{0.5}In_{0.5}Br_6$	2.17	$InBr_3$, LiBr, YBr_3	3.14	$InBr_3$, YBr_3, Br
$Li_3Sc_{0.5}In_{0.5}I_6$	1.98	$LiInI_4$, ScI_3, LiI	2.47	$LiInI_4$, ScI_3, I
$Li_3Sc_{0.5}Y_{0.5}I_6$	1.11	ScI_3, YI_3, LiI	2.47	ScI_3, YI_3, I
$Li_3Y_{0.5}In_{0.5}I_6$	1.98	$LiInI_4$, YI_3, LiI	2.47	$LiInI_4$, YI_3, I
$Li_3Sc_{0.5}In_{0.5}Cl_3Br_3$	2.17	LiCl, $InBr_3$, $ScCl_3$, LiBr	3.14	LiCl, $InBr_3$, $ScCl_3$, Br
$Li_3Sc_{0.5}Y_{0.5}Cl_3Br_3$	0.91	LiBr, YBr_3, LiCl, $ScCl_3$	3.14	YBr_3Cl, $ScCl_3$, Br
$Li_3In_{0.5}Y_{0.5}Cl_3Br_3$	2.17	LiCl, $InBr_3$, YBr_3	3.17	LiCl, $InBr_3$, YCl_3, Br
$Li_3Sc_{0.5}In_{0.5}Cl_3I_3$	1.98	$LiInI_4$, LiCl, LiI, $ScCl_3$	2.47	$LiInI_4Cl$, $ScCl_3$, I
$Li_3Sc_{0.5}Y_{0.5}Cl_3I_3$	0.97	LiCl, $ScCl_3$, LiI, YI_3	2.47	LiCl, $ScCl_3$, YI_3, I
$Li_3In_{0.5}Y_{0.5}Cl_3I_3$	2.04	InI_3, LiCl, YI_3	2.53	InI_3Cl, YCl_3, I
$Li_3Sc_{0.5}In_{0.5}Br_3I_3$	2.04	InI_3, LiBr, ScI_3	2.50	InI_3Br, $ScBr_3$, I
$Li_3Sc_{0.5}Y_{0.5}Br_3I_3$	1.11	LiBr, ScI_3, YI_3	2.50	LiBr, ScBr3, YI_3, I
$Li_3In_{0.5}Y_{0.5}Br_3I_3$	2.04	InI_3, LiBr, YI_3	2.50	InI_3Br, YBr_3, I

Table S4: DFT-PBE bandgaps (eV) of Li_3MX_6.

Halides	Bandgap(eV)
Li_3ScCl_6	3.72
Li_3YCl_6	4.85
Li_3InCl_6	3.65
Li_3ScBr_6	2.87
Li_3YBr_6	3.94
Li_3InBr_6	2.64
Li_3ScI_6	2.19
Li_3YI_6	3.01
Li_3InI_6	1.60
$Li_3ScCl_3Br_3$	2.89
$Li_3YCl_3Br_3$	4.03
$Li_3InCl_3Br_3$	2.68
$Li_3ScCl_3I_3$	2.00
$Li_3YCl_3I_3$	3.07
$Li_3InCl_3I_3$	1.62
$Li_3ScBr_3I_3$	2.05
$Li_3YBr_3I_3$	2.96
$Li_3InBr_3I_3$	1.68
$Li_3Sc_{0.5}In_{0.5}Cl_6$	3.73
$Li_3Sc_{0.5}Y_{0.5}Cl_6$	3.79
$Li_3Y_{0.5}In_{0.5}Cl_6$	3.75
$Li_3Sc_{0.5}In_{0.5}Br_6$	2.70
$Li_3Sc_{0.5}Y_{0.5}Br_6$	3.06
$Li_3Y_{0.5}In_{0.5}Br_6$	2.70
$Li_3Sc_{0.5}In_{0.5}I_6$	1.58
$Li_3Sc_{0.5}Y_{0.5}I_6$	2.26
$Li_3Y_{0.5}In_{0.5}I_6$	1.66

$Li_3Sc_{0.5}In_{0.5}Cl_3Br_3$	2.79
$Li_3Sc_{0.5}Y_{0.5}Cl_3Br_3$	2.94
$Li_3In_{0.5}Y_{0.5}Cl_3Br_3$	2.85
$Li_3Sc_{0.5}In_{0.5}Cl_3I_3$	1.63
$Li_3Sc_{0.5}Y_{0.5}Cl_3I_3$	2.14
$Li_3In_{0.5}Y_{0.5}Cl_3I_3$	1.66
$Li_3Sc_{0.5}In_{0.5}Br_3I_3$	1.63
$Li_3Sc_{0.5}Y_{0.5}Br_3I_3$	2.16
$Li_3In_{0.5}Y_{0.5}Br_3I_3$	1.67

Table S5: Minimum mutual reaction energies and phase equilibria of Li_3MX_6 toward typical cathode materials ($LiFePO_4$, $LiMn_2O_4$, $LiCoO_2$, $LiNiO_2$, $LiMnO_2$)

cathodes	Halides	Ratio xSE	Reaction energy (meV/atom)	Phase equilibria at xSE
$LiFePO_4$	Li_3ScCl_6	0.58	-35	$ScPO_4$, $Fe2PClO_4$, LiCl
	Li_3InCl_6	1.00	0	$LiFePO_4$
	Li_3ScBr_6	0.41	-34	$FeBr_2$, $ScPO_4$, LiBr
	Li_3InBr_6	0.00	-24	$InBr_3$, LiBr
	$Li_3ScCl_3Br_3$	0.58	-35	Fe_2PClO4, $ScPO_4$, LiBr, LiCl
	$Li_3Sc_{0.5}Y_{0.5}Cl_6$	0.58	-37	Fe_2PClO_4, YPO_4, $ScPO_4$, LiCl
	$Li_3Sc_{0.5}Y_{0.5}Br_6$	0.41	-38	$ScPO_4$, $FeBr_2$, YPO_4, LiBr
	$Li_3Sc_{0.5}Y_{0.5}Cl_3Br_3$	0.41	-40	$ScPO_4$, YPO_4, $FeBr_2$, LiBr, LiCl
$LiMn_2O_4$	Li_3ScCl_6	0.61	-27	$Sc_2Mn_2O_7$, $Mn_8Cl_3O_{10}$, MnO_2, LiCl
	Li_3InCl_6	0.89	-4	Mn_2O_3, $Li_5Mn_7O_{16}$, InClO, LiCl
	Li_3ScBr_6	0.34	-48	ScBrO, $Mn_{15}(Br_3O_{10})_2$, LiBr, Br
	Li_3InBr_6	0.00	-24	$InBr_3$, LiBr
	$Li_3ScCl_3Br_3$	0.34	-51	$Mn_{15}(Br_3O_{10})_2$, LiBr, ScBrO, BrCl, LiCl
	$Li_3Sc_{0.5}Y_{0.5}Cl_6$	0.44	-27	$Sc_2Mn_2O_7$, $Mn_8Cl_3O_{10}$, MnO_2, YCl_3, LiCl
	$Li_3Sc_{0.5}Y_{0.5}Br_6$	0.21	-43	ScBrO, $Mn_{15}(Br_3O_{10})_2$,

	$Li_3Sc_{0.5}Y_{0.5}Cl_3Br_3$	0.21	-47	LiBr, YBr_3, Br $Mn_{15}(Br_3O_{10})_2$, LiBr, ScBrO, BrCl, YBr_3, LiCl
$LiCoO_2$	Li_3ScCl_6	0.59	-48	$Li(CoO2)_2$, $Co_{23}O_{32}$, LiCl, Sc_2O_3
	Li_3InCl_6	0.50	-16	$Li(CoO_2)_2$, Co_3O_4, InClO, LiCl
	Li_3ScBr_6	0.17	-57	ScBrO, $CoBr_2$, LiBr, Br
	Li_3InBr_6	0.00	-24	$InBr_3$, LiBr
	$Li_3ScCl_3Br_3$	0.17	-61	ScBrO, $CoBr_2$, LiBr, BrCl, LiCl
	$Li_3Sc_{0.5}Y_{0.5}Cl_6$	0.54	-43	$Co_{23}O_{32}$, $Li(CoO_2)_2$, YClO, LiCl, Sc_2O_3
	$Li_3Sc_{0.5}Y_{0.5}Br_6$	0.23	-48	ScBrO, LiBr, Co_3O_4, YBr_3, Br
	$Li_3Sc_{0.5}Y_{0.5}Cl_3Br_3$	0.09	-52	$CoBr_2$, LiBr, ScBrO, BrCl, YBr_3, LiCl
$LiNiO_2$	Li_3ScCl_6	0.55	-122	$LiClO_4$, NiO, LiCl, Sc_2O_3
	Li_3InCl_6	0.55	-82	$LiClO_4$, In_2O_3, LiCl, NiO
	Li_3ScBr_6	0.27	-126	LiBr, Br_2O_3, $NiBr_2$, Sc_2O_3
	Li_3InBr_6	0.49	-43	Br_2O_3, In_2O_3, LiBr, NiO
	$Li_3ScCl_3Br_3$	0.29	-132	$NiBr_2$, $LiClO_4$, LiBr, LiCl, Sc_2O_3
	$Li_3Sc_{0.5}Y_{0.5}Cl_6$	0.50	-111	YClO, $LiClO_4$, NiO, LiCl, Sc_2O_3

	$Li_3Sc_{0.5}Y_{0.5}Br_6$	0.24	-107	YBrO, $NiBr_2$, LiBr, Br_2O_3, Sc_2O_3
	$Li_3Sc_{0.5}Y_{0.5}Cl_3Br_3$	0.25	-115	LiBr, $NiBr_2$, YClO, $LiClO_4$, LiCl, Sc_2O_3
$LiMnO_2$	Li_3ScCl_6	0.55	-85	Mn_2O_3, LiCl, Sc_2O_3
	Li_3InCl_6	0.55	-45	Mn_2O_3, In_2O_3, LiCl
	Li_3ScBr_6	0.47	-87	$Mn_{15}(Br_3O_{10})_2$, LiBr, Mn_3O_4, Sc_2O_3
	Li_3InBr_6	0.00	-24	$InBr_3$, LiBr
	$Li_3ScCl_3Br_3$	0.47	-88	$Mn_{15}(Br_3O_{10})_2$, LiBr, Mn_3O_4, LiCl, Sc_2O_3
	$Li_3Sc_{0.5}Y_{0.5}Cl_6$	0.53	-79	$Mn_8Cl_3O_{10}$, YMn_2O_5, Mn_3O_4, LiCl, Sc_2O_3
	$Li_3Sc_{0.5}Y_{0.5}Br_6$	0.54	-79	YMn_2O_5, $Mn_{15}(Br_3O_{10})_2$, Mn_3O_4, LiBr, Sc_2O_3
	$Li_3Sc_{0.5}Y_{0.5}Cl_3Br_3$	0.54	-80	YMn_2O_5, $Mn_{15}(Br_3O_{10})_2$, LiBr, Mn_3O_4, LiCl, Sc_2O_3

Table S6: Calculated activation energies (E_a) with errors and conductivity (σ) values and the reference for the eight identified candidates

Electrolytes	E_a (meV)	σ_{300K} (mS/cm)	Ref. E_a (meV)	Ref. σ_{300K} (mS/cm)	Ref.
Li_3ScCl_6	244.95 ± 18.73	6.515	270 ± 40	3.0	*eScience*, 2022, **2**, 79-86.
Li_3InCl_6	170.49 ± 31.37	76.654	190	20	*Acta Mater.*, 2024, **276**, 120135.
Li_3ScBr_6	235.93 ± 18.96	7.093	221	1.36	*J. Mater. Chem. C*, 2024, **12**, 4885-4896.
Li_3InBr_6	229.66 ± 35.30	7.678	\	\	\
$Li_3ScCl_3Br_3$	249.27 ± 17.45	5.204	\	\	\
$Li_3Sc_{0.5}Y_{0.5}Cl_6$	212.49 ± 19.99	14.348	\	\	\
$Li_3Sc_{0.5}Y_{0.5}Br_6$	321.41 ± 29.68	0.722	320 ± 50	0.58	*eScience*, 2022, **2**, 79-86.
$Li_3Sc_{0.5}Y_{0.5}Cl_3Br_3$	234.69 ± 12.37	8.841	\	\	\

Table S7: Input features for SHAP analysis.

Symbols	Features
S_{vib}	Li-ion vibrational entropy
S_2	Li-ion two-body entropy
$\bar{\omega}$	Li phonon band center
f_{Li-Li}	Li-Li strength
f_{Li-X}	Li-X strength
CSM	Li-anion polyhedron distortion degree
V	Anion sublattice volume
q_X	Anion charge
q_{Li}	Li charge

Table S8: Calculated diffusivity (D) with different number of time origins (N_{origin}) in Li_3ScCl_6 at 500K and 1000K.

N_{origin}	D at 500K ($\times 10^{-6}$ cm^2s^{-1})	D at 1000K ($\times 10^{-5}$ cm^2s^{-1})
1	4.31	5.35
5	4.47	5.35
10	4.51	5.34
50	3.35	5.37
100	4.35	5.37
200	4.35	5.37

Supporting Note 1: Determination of the time origins for MSD calculation from MD trajectory

The Li-ion MSD with varying numbers of time origins (N_{origin}) was calculated using the Li_3ScCl_6 MD trajectory at 500K and 1000K, following the equation from reference (*Comput. Phys. Commun.,* 2026, **320**, 109982.):

$$MSD = \frac{1}{N_j N_{origin}} \sum_{j=1}^{N_j} \sum_{i=1}^{N_{origin}} \langle \left| \vec{r}_j(\tau + t_i) - \vec{r}_j(t_i) \right|^2 \rangle,$$

where $\vec{r}_j(\tau + t_i)$ is the j-th atom position at time $\tau + t_i$, and N_j is the total number of atoms of element j in the simulation cell. N_{origin} is the number of time origins used for calculation of MSD and the symbol $\langle\ \rangle$ represents the ensemble average.

As shown in the newly plotted Figure S12, the MSD profile exhibits statistical noise at smaller N_{origin} values. However, as N_{origin} increases to 50, the MSD-t curve smooths and the extracted Li-ion diffusivity converges (as summarized in Table S8). Because the simulation supercells contain a number of mobile Li-ions, ensemble averaging mitigated the statistical noise (*J. Appl. Phys.*, 2015, **117**, 4). As a result, the diffusivities obtained from our single-origin analysis show only a negligible discrepancy when compared to the strictly converged values at N_{origin}=50. The extracted diffusivities were based on the raw trajectory data utilizing a single time origin (N_{origin}=1)which balance the fitted data robust and computational efficiency.

Supporting Note 2: Discussion on balancing the trade-off between reduced electrochemical stability and entropy-driven gains.

The trade-off between electrochemical stability and ionic conductivity is a known challenge in solid electrolyte design. As shown in Figure 2(b) of the manuscript, the electrochemical oxidation limit is determined by the valence band maximum (VBM). In mixed-halide systems, the VBM is dictated by the least electronegative anion, where introducing a small fraction of I or Br reduces the oxidation potential. Conversely, the entropy-driven performance gain relies on the overall structural disorder created by the mixed local environments, rather than the properties of a single element.

Regarding anion mixing, incorporating bromide presents a pragmatic compromise to balance the trade-off between reduced electrochemical stability and entropy-driven gains due to its moderate lattice softening and intermediate oxidation potential. For example, comparing Li_3YCl_6 (E_a=278meV), $Li_3YCl_3Br_3$ (E_a=223meV), and $Li_3YCl_3I_3$ (E_a=201meV) shows that while $Li_3YCl_3I_3$ exhibits the lowest activation energy, the incorporation of iodine induces a drastic penalty to the oxidation potential (decreasing to 2.53 V) compared to $Li_3YCl_3Br_3$ (3.13 V). Because electrochemical stability is limited by the least electronegative anion while diffusion improves via softening and disordering, anion mixing could result in a performance trade-off.

Supporting Note 3: Discussion on the relationship between attempt frequency and the entropy.

According to the stochastic random walk model, the ion diffusion coefficient is expressed as $D = \frac{1}{2d}\lambda^2 v_0 \exp\left(-\frac{\Delta G_m}{k_B T}\right)$, where λ is the ion hopping distance, v_0 is the attempt frequency, and d represents the number of dimensions considered in the migration process. Here, we employ natural logarithm of pre-index factor of ion diffusion coefficient (lnD_0) as a proxy for the attempt frequency (v_0). (*J. Solid State Chem.*, 1972, **4**, 294-310.) As Figure S13 shows, high S_{vib} and S_2 seem to be correlated with low D_0. A more comprehensive understanding is still needed with more data and analyses to uncover which aspect of spectrum affect attempt frequency more.

Supporting Note 4: Details of the definition of full width at half maximum (FWHM).

The raw Li VDOS data are fitted by a normal (Gaussian) distribution function:

$$f(\omega) = \frac{1}{\sigma\sqrt{2\pi}} \exp\left(-\frac{(\omega-\mu)^2}{2\sigma^2}\right),$$

where μ determines the peak position and σ is the standard deviation that governs the profile shape. Once σ is extracted from the fit, the FWHM is analytically calculated using the standard mathematical relation for a Gaussian peak:

$$FWHM = 2\sqrt{2\ln 2}\ \sigma \approx 2.355\sigma.$$

The fitted curves with the raw VDOS profiles for 4 representative halides are shown in Figure S14, the Gaussian function captures the dominant broadening behavior. For the 36 halides analyzed, the average fitting R^2 is close to unity (0.98), confirming that the single-peak approximation is highly acceptable for our systems.

Supporting Note 5: Effects of mixed-ion with non-equimolar compositions and multi-principal elements on Li diffusion

To evaluate the phenomenon in the C2/m Li_3MX_6 halide framework with non-equimolar compositions, we calculated the Li-ion activation energy (E_a) and the corresponding entropy descriptors (S_2 and S_{vib}) for the $Li_3Sc_{1/2}Y_{1/2}Cl_6$, $Li_3Sc_{1/3}Y_{2/3}Cl_6$, $Li_3Sc_{1/3}Y_{1/3}In_{1/3}Cl_6$. As shown in the Figure S15, the binary equimolar system yields higher S_2 and S_{vib}, and a lower activation energy, than the non-equimolar one. Furthermore, comparing the ternary ($Li_3Sc_{1/3}Y_{1/3}In_{1/3}Cl_6$) and binary ($Li_3Sc_{1/2}Y_{1/2}Cl_6$) equimolar systems reveals that although the ternary system possesses the highest ideal configurational entropy, it exhibits lower S_2 and S_{vib}, leading to a higher E_a. Parameter analysis indicates that incorporating a third cation (In) induces local chemical heterogeneity and restricts localized structural disorder (evidenced by a sharper first peak in the RDF). This observation demonstrates that higher configurational entropy upon multi-element mixing may not necessarily reduce the activation energy, which will be dependent on the changes in S_2 and S_{vib}.